Microchemical Journal 194 (2023) 109297

Contents lists available at ScienceDirect

Microchemical Journal

journal homepage: www.elsevier.com/locate/microc

Preparation and Characterization of Fe-Gallic acid MOF for determination of antiviral Molnupiravir as inhibitor for RNA Corona virus replication

Huda M. Younis [a], A.O. Youssef [b], Said M. El-Sheikh [c,*], Sheta M. Sheta [d,*], Mohamed S. Attia [b,*]

[a] College of Dentistry, University of Basrah, Iraq
[b] Chemistry Department, Faculty of Science, Ain Shams University, Abbassia 11566, Cairo, Egypt
[c] Department of Nanomaterials and Nanotechnology, Central Metallurgical R & D Institute, Cairo, 11421, Egypt
[d] Department of Inorganic Chemistry, National Research Centre, 33 El-Behouth St., Dokki, Giza, 12622, Egypt

ARTICLE INFO

Keywords:
Gallic acid
Fe-Gallic acid MOF
Fluorescence
Quenching
Molnupiravir

ABSTRACT

Fe-Gallic acid metal organic framework (MOF) was synthetized and characterized by acquired qualitative and quantitative micro analytical tools such as: FE-SEM/EDX, XPS analysis, XRD analysis, FT-IR, and Fluorescence spectroscopy. Fe-Gallic acid MOF is used as a sensor for the determination of antiviral Molnupiravir (MOL) in pharmaceutical formulations, urine and serum samples. The existence of adequate functional groups in (MOL) solution in DMSO induces the interaction with the Fe- Gallic acid MOF complex that absorb energy at the characteristic wavelength of the organic ligand (λ_{ex} = 290 nm) and emits radiation at 357 nm over a working range of $1 \times 10^{-5} - 1 \times 10^{-9}$ mol/L. The Fe-Gallic acid MOF sensor is a sensitive and cost-effective method for the detection of Molnupiravir. It has a detection limit of 2.24×10^{-9} mol/L, which is lower than other methods for the detection of Molnupiravir. The Fe-Gallic acid MOF sensor is also easy to use and does not require any special equipment. It is a promising new method for the detection of Molnupiravir, and it could be used in a variety of settings, including clinical laboratories and point-of-care settings.

1. Introduction

The Immediate intervention with confirmed COVID-19 patients with mild symptoms can effectively diminish the progress to severe symptoms and hospitalization. Among the suggested promising treatments is Molnupiravir (MOL) which is considered one of the portentous antiviral agents that could minimize the risk of hospitalization and death rates in non-hospitalized COVID-19 patients. MOL proved to be most effective against infections with existing and potential emerging SARS-CoV-2 variants of concern (VoCs) [1–4]. The effectiveness data have been widely described in COVID-19 patients [5–10]. MOL, N-Hydroxy-5′-O-isobutyryl-3,4-dihydrocytidine [(2R,3S,4R,5R)-3,4-Dihydroxy-5-[4-(hydroxyamino)-2-oxopyrimidin-1-yl] oxolan-2-yl] methyl 2-methyl-propanoate, is a prodrug metabolized to the ribonucleoside analogue N-hydroxycytidine (NHC) which circulates into cells, then phosphorylated to generate the pharmacologically active ribonucleoside triphosphate (NHC-TP). Its mechanism of action is recognized through a viral error catastrophe where the NHC-TP inclusion into viral RNA by the viral RNA polymerase, results in a buildup of errors in the viral genome that will lead to the discontinuation of replication [11–15]. MOL could be counted as the first oral, direct-acting antiviral with a pronounced efficiency in decreasing the nasopharyngeal SARS-CoV-2 infectious virus and viral RNA while exhibiting a promising safety and tolerability reports [16–19]. The chemical structure of MOL is shown in S 1. Few analytical methods for MOL determination have been found in the literature review. Levels of MOL in human plasma have been measured using liquid chromatography coupled with tandem mass spectrometry (LC-MS/MS) [17] and in hamster model [20]. However, the validation details have not been fully defined or reported except for the LC-MS/MS determination of MOL and its metabolite in human plasma and saliva [21]. Metal-organic frameworks (MOFs) are crystalline porous materials with a high degree of both compositional and structural control. MOFs are composed of metals ions or groups coordinated with organic bonds forming one or multidimensional structures [22]. Luminescent metal organic frameworks (LMOFs) class is considered one of the most widely employed MOFs especially for diagnostic purposes owing to their peculiar optical features. This newly evolving class of LMOFs, constructed through metal connecting nodes together with bridging ligands and linkers are emerged as a promising and reliable approach towards quick monitoring of some bioactive moieties. Owing to the adaptable

* Corresponding authors.
E-mail addresses: selsheikh2001@gmail.com (S.M. El-Sheikh), dr.sheta.nrc@gmail.com (S.M. Sheta), Mohamed_sam@yahoo.com (M.S. Attia).

https://doi.org/10.1016/j.microc.2023.109297
Received 21 May 2023; Received in revised form 29 August 2023; Accepted 30 August 2023
Available online 3 September 2023

nature of LMOF building units, the source of fluorescence could be from both metal centers and ligand within the LMOFs. In addition, the optical features could be regulated through the interactions between the building blocks. Moreover, some photo responsive constituents could be integrated into the LMOFs structure to induce additional florescence apart from that originated from the LMOFs subunits to open the door for unlimited applications in clinical ailment diagnosis and treatment effectiveness. Interestingly, the fluorescent responses and sensitivities of LMOFs are mostly dependent on the fluorescence modifications driven by electron-energy transfer between the targeted biological molecules and the corresponding LMOFs. In this aspect, the reversible pre-concentration of the targeted molecules is facilitated by the intrinsic porosity and tunable functional sites in LMOFs, which in turn would boost the detection selectivity and specificity [23–31]. LMOFs structural composition in combination with the energy conversion (ET) specifications could be easily tuned [32–37]. The LMOF based biosensors mainly operate through different mechanisms, including quenching and enhancement of the luminescent responses known as turn-off and turn-on responses, respectively, [38–51]. In this study, Fe-Gallic acid MOF was synthesized and characterized by acquired qualitative and quantitative micro analytical tools. Fe-Gallic acid MOF was then used as a sensor for the determination of MOL in pharmaceutical formulations and serum samples. The results showed that Fe-Gallic acid MOF is a sensitive and selective sensor for MOL, and it could be used to detect MOL in a variety of samples. This study is a promising step towards the development of a rapid and accurate method for the determination of MOL in clinical samples. Molnupiravir is a promising new antiviral agent, and the development of a rapid and accurate method for its determination could help to improve the management of COVID-19.

2. Materials and reagents

3,4,5-Trihydroxybenzoic acid (Gallic acid) $(HO)_3C_6H_2COOH$, 99.0%; and iron(III) sulfate hydrate $Fe_2(SO_4)_3{\cdot}5H_2O$, 97.0%, were purchased from Sigma Aldrich. All other chemical and reagents are of analytical grade and were used without further purification. All materials used are of analytical-reagent of higher grade. MOL, purity (98%), was obtained from Optimus Drugs Pvt LTD, India. (MOL 200 mg per capsule, R&D prepared samples) was used as pharmaceutical formulation dosage form. American Society for Testing and Materials (ASTM) grade I water, was daily obtained from the central laboratory. Potassium dihydrogen phosphate, sodium dihydrogen phosphate, dipotassium hydrogen phosphate, *o*-phosphoric acid, acetic acid, sodium acetate anhydrous, were supplied by Scharlau, Barcelona, Spain. A standard stock solution of MOL was prepared and diluted to form a working (1.0×10^{-5} mol/L) MOL using DMSO. Pharmaceutical preparation of hard capsule MOL containing 200 mg of MOL per capsule produced EVA PHARMA, EGYPT.

2.1. Synthesis of Fe(III)-GA-MOF

The MOF synthesis was performed through a simple reaction of $Fe_2(SO_4)_3{\cdot}5H_2O$ (3.0 mmol, 1.470 g) dissolved in 50 mL distilled water/DMF (3:2 V/V, respectively), which added dropwise to round flask containing gallic acid (1.0 mmol, 0.170 g) dissolved in distilled water, with continues stirring. Then, the reaction mixture was refluxed for 48 h at 80 °C. A dark brown black precipitate was formed then filtrated and washed with distilled water and ethanol..

2.2. Instruments

All fluorescence measurements were recorded with a Meslo-PN (222–263000) Thermo Scientific Lumina fluorescence Spectrometer in the range (190–900 nm). The absorption spectra are recorded with Thremo UV–Visible double-beam spectrophotometer. All pH measurements are made with a pHs-Janway 3040 ion analyzer.

2.3. General procedure

A mixture of 0.01 mL (1.0×10^{-2} mol/L) MOL and 0.01 mL (1.0×10^{-2} mol/L) Fe-Gallic acid MOF was prepared and diluted to the mark with DMSO in a 10 mL measuring flask and kept for 15 min before use. The preceding optical sensor is utilized to obtain the subsequent measurements of absorption and emission spectra and study the effect of pH and solvents where the corresponding luminescence intensity was measured at $\lambda_{ex}/\lambda_{em} = 290/352$ nm.

2.4. Calibration curve

After mixing Fe-Gallic acid MOF with a series of 1.0×10^{-5} to 1.0×10^{-9} mol/L concentrations of MOL in 10 mL measuring flasks prepared from 1.0×10^{-2} mol/L stock solution, the luminescence spectra were measured accordingly in the cell of spectrofluorometric device at the specific excitation wavelength $\lambda_{ex} = 290$ nm. The solution in the cell must be rinsed after each measurement by DMSO.

2.5. Validation

2.5.1. Accuracy and precision

Hard capsules MOL are used at two different concentrations (1.0×10^{-7} and 1.0×10^{-8}) mol/L of the optical sensor to determine the repeatability (intra-day precision) three times with in the day and the intermediate (inter-day precision) three times on different days of the intended method. The results were summarized in Table 2. The percentage of the obtained relative standard deviation (%RSD) values were 1.29–1.19% (intra-day) and 1.13– 1.11% (inter-day) for hard capsule MOL which reflects the high precision of the study. A high accuracy was calculated as percentage relative error (RE) for the measured mean concentration and the taken concentration of MOL.

2.5.2. Selectivity

The synthetic mixture and a placebo blank of MOL consisting of interfering substances as cellulose (40 mg), starch (30), lactose (50 mg), povidone (200 mg), and sodium starch glycolate (50 mg), magnesium stearate (20 mg) were analyzed to scrutinize the method selectivity. No influence on the luminescence spectrum was recorded by the excipients that were extracted and tested as reported by the proposed procedure. A competitive analysis for the synthetic mixture of MOL was implemented. A combination between an identical component of the placebo blank and discrete concentrations of MOL solution was formed.

2.5.3. Determination of Molnupiravir in pharmaceutical preparations

Two distinct concentrations of 1.0×10^{-6} mol/L and 1.0×10^{-7} mol/L mol were developed in 10 mL flasks by grinding two MOL hard capsules and then dissolving them in acetonitrile. Filter the MOL solution and separate the insoluble materials from the filtrate. The concentration of Molnupiravir in the filtrate was determined using a high-performance liquid chromatography (HPLC) assay. Briefly; the capsule is crushed and the powder is dissolved in acetonitrile. The solution is injected into the HPLC instrument. The solution is passed through a column filled with a substance that selectively binds to Molnupiravir. Molnupiravir is removed from the column and detected with a detector. The amount of Molnupiravir was determined by comparing its peak height or area with the peak height or area of a standard Molnupiravir solution. The concentration of Molnupiravir was found to be 1.2×10^{-3} mol/L. Take 5 mL of this filtrate and dilute it with 95 mL DMSO (6.0×10^{-5} mol/L). Then combine 0.16 mL of this solution with 1.0 mL of 10^{-4} mol/L Fe-Gallic acid MOF in a 10 mL measuring flask and supplement to the mark with DMSO. Composite optical sensors were used to confirm the validation of the current technique by recording the fluorescence intensity and comparing it to similar concentrations in the calibration graph.

2.5.4. Determination of Molnupiravir in real serum and urine samples

A serum and urine samples have been taken after three hours from a COVID-19 patient was taken a dose of one capsule. Blood sample is collected in a tube containing an anticoagulant such as heparin or EDTA. The sample is then centrifuged to separate serum from the blood cells. The urine sample is centrifuged to remove any particles or debris. Serum and urine samples are used directly for analysis. (The serum and urine samples may be diluted with a suitable buffer or solvent to achieve the desired concentration range for analysis).

3. Results and discussion

3.1. Characterization of Gallic-Fe MOF

The Fe(III)-GA-MOF was prepared via a simple reaction of 3.0 mmol of iron(III) sulfate pentahydrate with 1.0 mmol gallic acid. A dark brown black precipitate was obtained as obtained [52–54], the precipitate was filtered, then washed and dried well under vacuum. The structure elucidation using the acquired qualitative and quantitative micro analytical tools was discussed herein below:

3.1.1. FE-SEM/EDX

The Fe(III)-GA-MOF FE-SEM images at different magnifications were represented in (Fig. 1a–c). The morphology appears to be an aggregates of broken brick blocks with smooth surface. The upper surface is homogenized and formed from a small nanoparticle. Whereas, the Fe(III)-GA-MOF EDX-analysis presented (Fig. 1d). The data displayed the presence of oxygen, carbon, sulphur and iron as a block element building of the structure. The tremendous dispersion of the concert elements through the cross-section revealed by mapping-analysis (Fig. 1d) is confirms the Fe(III)-GA-MOF formation.[52].

3.1.2. XPS analysis

The Fe(III)-GA-MOF chemical components was characterized using XPS, Fig. 2. The data obtained are in a good agreement with the published XPS data in the literature [52,54].The four main spectral parts of this sample were analyzed using the XPS wide spectral survey. The XPS scan presented in Fig. 2a and S 2 exhibited clearly detected peaks of iron (Fe 2p), oxygen (O 1 s), carbon (C 1 s) and sulfur (S 2p). Fe 2p peak was deconvoluted into six spectral peaks as shown in Figure 2b and S 3. The six spectral peaks were observed at binding energies of 710.66, 714.38, 718.14, 723.96, 725.59 and 728.24 eV, due to Fe $2p_{1/2}$ and Fe $2p_{3/2}$, for Fe (III) and Fe (II). The most abundant Fe(III) satellite peaks at 710.66 eV and 723.96 eV which confirmed the Fe^{3+} extinction of Fe(III) $2p_{3/2}$ and Fe(III) $2p_{1/2}$, respectively with a decreasing energy difference of 13.3 eV [55]. Fig. 2c and S 4 presented the spectrum of the detuned O 1 s peaks at 531.73, 532.69 and 533.12 eV [56]. Fig. 2d and S 5 show the C 1 s region, with spectral peaks at 288.60, 286.38 and 284.75 eV assigned to C = O, C = C and C-O respectively [57]. Finally, Fig. 2e and S 6 present the S 2p spectrum and it shows one peak at 168.89 eV due to the presence of sulfur in the sample. S 6 contained more detailed information about XPS analysis.

3.1.3. XRD analysis

The Fe(III)-GA-MOF XRD spectrum (powder) pattern was represented in (Fig. 2f). The XRD pattern of the Fe–GA were consistent with the reported XRD of GA/FeIII MOFs [52–54,58,59] as obtained in the inserted Fig. 2f. The XRD patterns showed no sharp peaks of the MOF confirming that the amorphous phase of the material is formed. Moreover, the main peaks in the diffraction pattern of the Fe(III)-GA-MOF were observed at 2θ values of about 9.24°, 11.34°, 27.5°, 29.88°, 38.34°, 45.13°, 56.44°, 58.63°, 61.45°. The details of XRD analysis peaks list of the Fe(III)-GA-MOF was presented in (S 8). Additionally, the diffraction pattern of the Fe(III)-GA-MOF was in a good agreement with MOFs-based gallic patterns.

3.1.4. FT-IR spectrum

The FTIR spectrum of Fe–GA MOF was similar to that of Fe–GA in the literature [52,53] FT-IR spectrum of the Fe(III)-GA-MOF is shown in (Fig. 3) in compared with FT-IR spectrum of the GA (Inserted in Fig:3). From this (Fig. 3), it can conclude that: the main characteristic bands of gallic acid appeared for the hydroxyl (O-H) stretching at 3407.05 and 3269.11 cm^{-1} [phenolic ν(OH) at 3407.05 cm^{-1} and carboxyl ν(OH)) at 3269.11 cm^{-1}], and C = O stretching at 1612.39 cm^{-1} [60]. In addition to the other major peaks that appeared at 3064.91, 2654.68, 1540.11, 1438.27, 1200.67, 1100.09, 1045.14, 762.25, 699.25, 567.87, 553.80, 466.88 cm^{-1} [61]**.** The characteristic bands: a band near 3200 cm^{-1} due to the O-H axial deformation and 3100 cm^{-1} due to the aromatic C-H

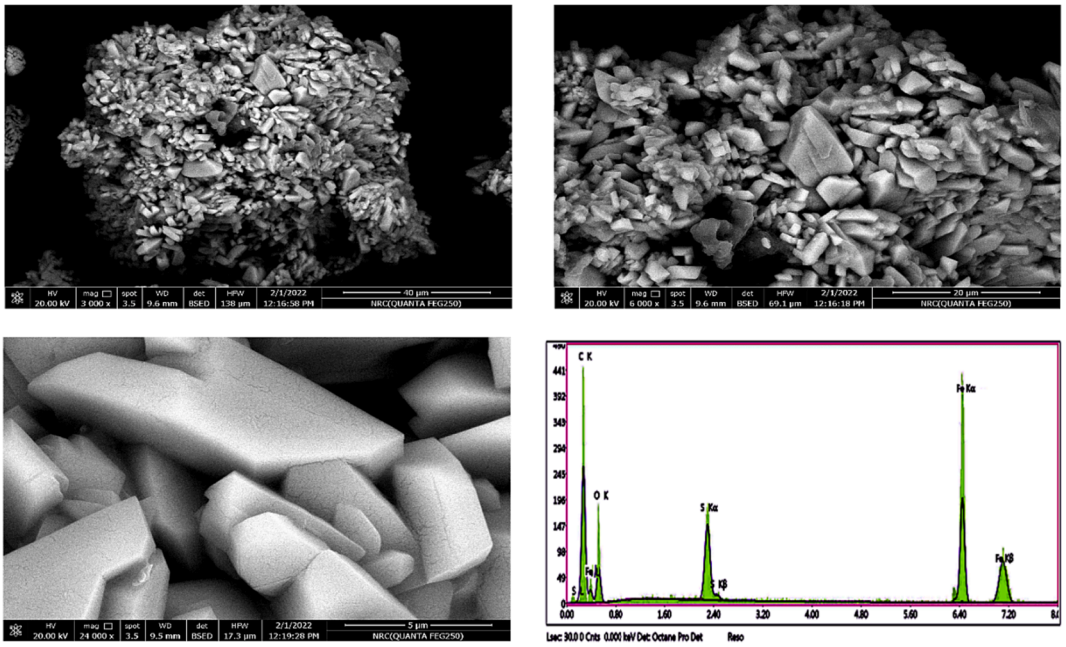

Fig. 1. (a, b, and c) The field-emission scanning electron microscopy images of the ferric metal–organic framework (Fe(III)-GA-MOF) at different magnification, and (d) Energy-dispersive X-ray analysis with a single point EDX mapping analysis of Fe(III)-GA-MOF.

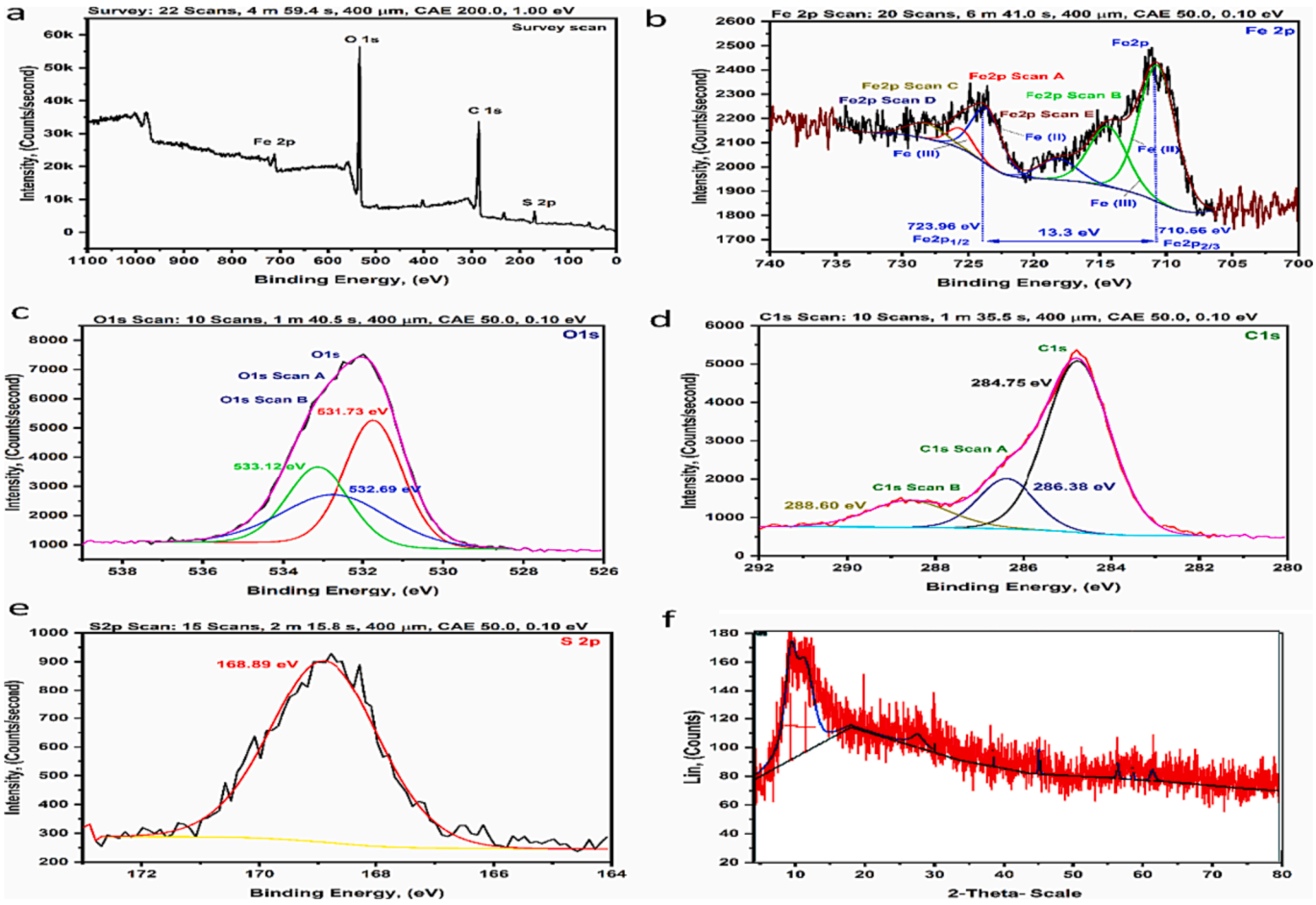

Fig. 2. (a–e) The XPS analysis of the Fe(III)-GA-MOF: [(a) Survey, (b) Fe 2p, (c) O 1 s, (d) C 1 s, (e) S 2p], (f) The X-ray diffraction spectra of the Fe(III)-GA-MOF.

axial deformation; the appearance of a band at 1700 cm^{-1} represented the C = O axial deformation; the C = C axial deformation in aromatics appeared around 1600 and 1500 cm^{-1} while the band at 1350 cm^{-1} indicated the O-H deformation; 1250 cm^{-1} the C-O axial deformation and 650 cm^{-1} the C-H axial deformation in aromatics. On the other hand, in the FT-IR spectrum of the Fe(III)-GA-MOF are observed that the bands of hydroxyl (O-H) (the phenolic ν(OH) at 3407.05 cm^{-1} and carboxyl ν(OH)) at 3269.11 cm^{-1}) are disappeared due to complexation to Fe ion. The two coordination possibilities for the iron ion and gallic acid occur through the phenolic hydroxyl and the carboxyl groups. With the formation of the Fe(III)-GA-MOF and complexation with iron, a decrease in the intensities of the GA bands are observed. The decrease in the peak's intensities due to the complexation with transition metals, the metal ions can accept both σ electrons from the ligand as well as π electrons from the aromatic ring when filling the d orbitals available for coordination. On the other hand, no differences were observed between the peaks in the regions between 1200 and 720 cm^{-1} for the C-H bonds angular deformations in the aromatic ring. The peak revealed at 1107 cm^{-1} is assigned to Fe-O-Fe [62]. The band appears at 590.85 and 476.79 cm^{-1} assigned to the ferric ions-oxygen coordination and covalent bonding [ν(Fe–O)] and [ν(Fe < − O)], respectively. The last above two bands confirm the chelation of the ferric ion with GA by the O atoms [63a–d, 64,]. Fig. (S 9) represented the published data about(a) Crystal structure of gallate-based metal–organic frameworks (MOFs) [52,53], (b) Ball-and-stick rendering of Fe($C_7O_5H_3$)·3.22 H_2O complex showing coordination of the gallate ligand [52,54], (c) Structure of the Fe(III) octahedral pyrogallin complex (Fe2($C_6O_3H_3$)2·•4H_2O) proposed by Krekel [54]. (d) 3D Structural representation of the Fe(III)-GA-MOF monomeric unit. e) of GA for the GA/FeIII system (coordination modes are based on Refs. [55,65,66]. In view of the physical and spectral results discussed in the above addition to the published data, it can be assumed the monomeric unit 3D structure of the Fe(III)-GA-MOF as presented in (S 9 (d)).

3.2. Spectral characteristics

GA-based MOFs exhibit luminescence/sensing properties due to their p-bonded systems and low energy LUMO (p*) in the GA bond, thus GA-based MOFs are effective for sensing. Furthermore, these host frameworks have the ability to selectively and efficiently interact with the target analyte to act as a fluorophore due to their free base sites. Once the receptor has recognized the analyte, fluorescence signals can be observed in the form of quenching due to either electron transfer (ET), charge transfer (CT), or energy transfer processes. [67] The M^{2+} ion with d^{10} formation is difficult to oxidize or reduce, primarily resulting in localized ligand emission caused by p-p* and/or n-p* transitions of the conjugates, whereas metal-to-ligand charge transfer contribution (MLCT) or Ligand charge to metal charge transfer (LMCT) is negligible in emission. Therefore, the luminescent emission band of the metal complex can be assigned to the intra-ligand emission, and the luminescent enhancement is attributed to the coordination bonds between M^{2+} and the ligand, which adjust the conformational rigidity of the ligands and cause a decrease in non-radiative shift elements. While in the case of ferromagnetic M^{3+} (Fe^{3+}, d^5) the contribution of metal-to-ligand charge transfer (MLCT) or ligand-to-metal charge transfer (LMCT) predominates in the emissions. Paramagnetic transition metal complexes typically show weak emission, where their partially filled orbitals producing d–d ligand domain transitions may lead to strong reabsorption

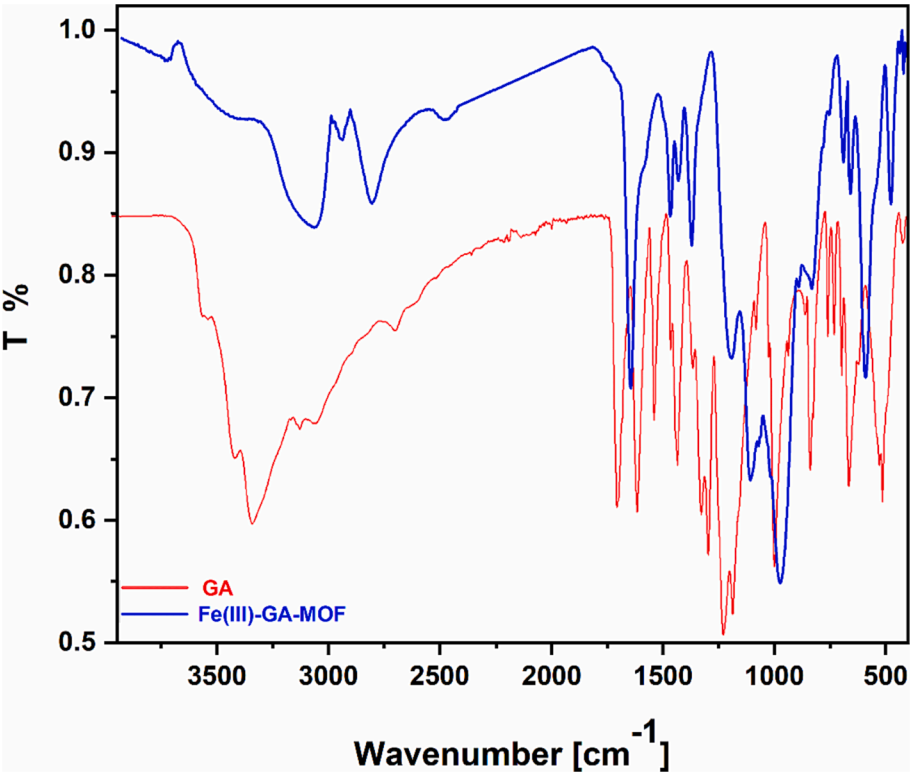

Fig. 3. The FT-IR spectrum of Fe(III)-GA-MOF in compared with GA- FT-IR spectrum.

and/or fluorescence suppression of organic molecules via electron or energy transfer. The resulting emission depends on the nature of the MOF structure, such as the spacing and orientation between the junctions, the HOMO-LUMO gap of the junctions versus the accessible states of the metallic units, the electronic configuration of the metal, and the bonding geometry. [68,69] Luminescence from MOFs containing transition metal ions in the framework is usually centered on the linker, but can also involve metal ion perturbation on the linkers or even modulate charge transfer between the metal and the linker. [66] The emission spectrum of gallic acid shows major peaks at 341 nm, which can be attributed to the p*-p shift, (S 10a). [65] In complexation with M^{3+} metal ions (Fe^{3+}), the emission spectra of the frameworks show emissions at about 357 nm (λ_{ex} = 290 nm), (S 10b). The emission spectra of the Fe-GA MOF shows strong emission in aprotic solvents such as; DMSO, acetonitrile and DMF, while showing lower emission intensities in protic solvents such as water and ethanol, (S 10b). The response of the luminescent signal of the sensor is directly related to the change of pH of the solvent. The optimal fluorescent intensity was recorded at pH = 8.8. Therefore, 0.1 mol/L of NH_4OH was used before each measurement to obtain a pH of 8.8. (S11). [70–82].

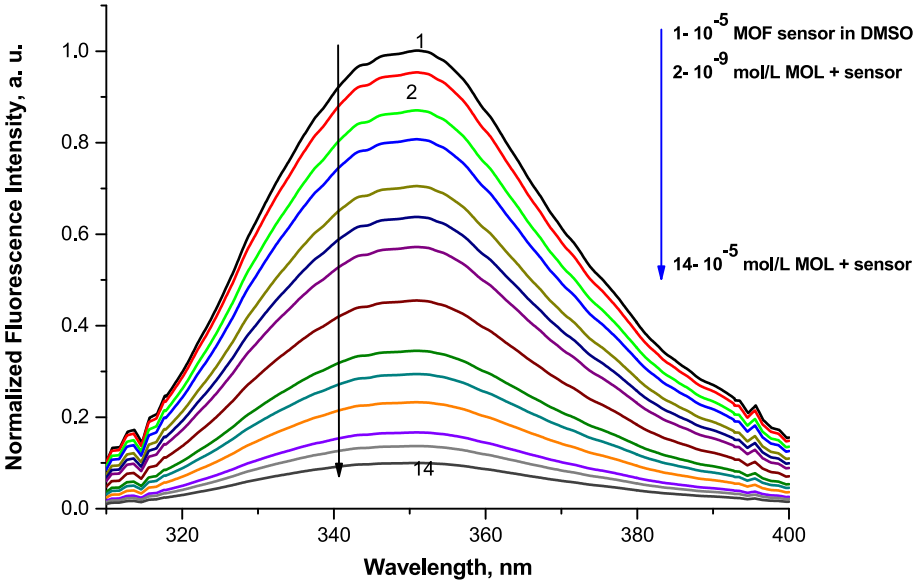

Fig. 4a. Emission spectra of fe-ga mof in different concentrations of mol.

3.3. Linear range and limit of detection

A linear relationship was obtained between the concentration of Molnupiravir and the peak intensity of the Fe-Ga MOF at 351 nm, and this correlation was found to be linear within the concentration range from 1×10^{-9} to 1×10^{-6} mol/L. Fig. 4a and b. Correlation was obtained by applying a Stern-Volmer plot, which yielded a Stern-Volmer constant (κ_{sv}) of 3.1 $mol^{-1}L$ and a critical concentration of molnopiravir (C_o) of 2.49×10^{-10} mol. L^{-1}. The distance between Molnupiravir and Ionophore was found to be 2.16 Å, which indicates an electron transfer mechanism for quenching. Regression equations were calculated, and regression parameters were computed, including the limit of detection (LOD) and limit of quantification (LOQ), which were determined using the formulas LOD = 3.3 S/b and LOQ = 10 S/b, where S is the standard deviation of the intensity values luminescence blank, and b is the slope of the calibration plot [83,84]. The LOD and LOQ values are recorded in Table 1. The method was found to be sensitive, with a suitable working range of $1 \times 10^{-6} - 1 \times 10^{-9}$ mol/L.

3.4. Selectivity

The proposed method for the determination of Molnupiravir in pharmaceutical formulations, urine, and serum samples are selective and accurate. The method was tested by analyzing a placebo blank containing inactive ingredients and a synthetic mixture of Molnupiravir and the inactive ingredients. The placebo blank analysis showed that there was no interference from the inactive ingredients. The synthetic mixture analysis showed that the proposed methods were able to accurately determine the concentration of Molnupiravir in the mixture. The percent recovery of Molnupiravir was 99.50 ± 0.65, 99.9 ± 1.75, and 99.60 ± 0.80 for pharmaceutical formulations, urine, and serum samples, respectively. These results suggest that the proposed method is accurate and precise for the determination of Molnupiravir in a variety of samples.

3.5. Application to pharmaceutical formulation and real samples

The proposed method for the determination of Molnupiravir in hard capsule Molnupiravir is successful and accurate. The method was tested by analyzing hard capsule Molnupiravir, the results in Table 2 showed that the method was able to accurately determine the concentration of Molnupiravir in the pharmaceutical sample. The R.S.D for the tablet in the proposed method is (1.43 %). The R.S.D for the tablet sample in the B.P method is (0.1 %). The results obtained by the proposed method agree well with those of reference method as well as with the label claimed, Table 2. The method was tested also by analyzing a serum and urine samples have been taken after three hours from a patient was taken a dose of one capsule. The results were reported in Table 2, in which the RSD % for serum and urine samples is 1.2% and 1.8 %, respectively.

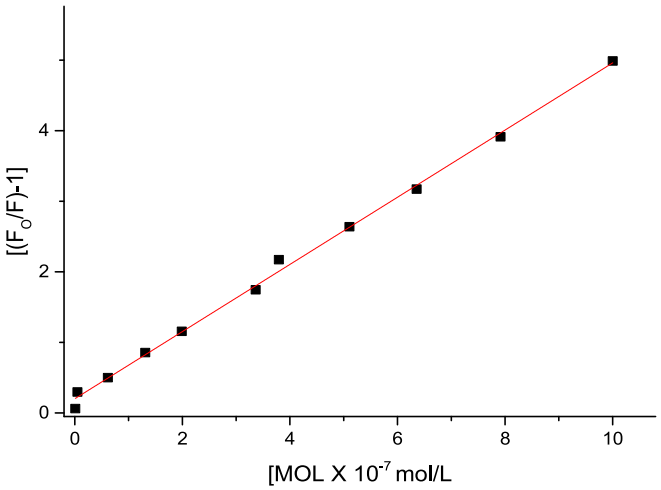

Fig. 4b. Linear relationship between [f_O/F-1] against [MOL].

Table 1
Sensitivity and regression parameters for photo probe.

Parameter	*value*
λ_{em} *nm*	351
Linear range, mol/L	$1.0 \times 10^{-6} - 1.0 \times 10^{-9}$
Limit of detection (LOD), mol/L	2.24×10^{-9}
Limit of quantification (LOQ), mol/L	7.39×10^{-9}
*Regression equation, Y**	Y = bX
Intercept (a)	0.203
Slope (b)	0.47×10^{7}
Standard deviation	0.008
Variance (Sa^2)x 10^{-5}	6.4
Regression coefficient (r)	0.997

*Where Y = [(F_0/F)-1], X = concentration in mol/L, a = intercept, b = slope.

Table 2
Results of repeatability study.

Samples	standard method*	Proposed method	Pure MOL recovered (Percent ± SD)
MOL 200 mg per capsule	0.10	0.102	102.0 ± 1.25
[MOL] $\times 10^{-7}$ mol/L	1.00	0.980	98.00 ± 1.45
Urine sample (real) µmol	0.53	0.525	99.0 ± 1.2
Serum sample (real) µmol	0.52	0.514	98.8 ± 1.80

* British Pharmacopeia.

3.6. Repeatability and reproducibility

Repeatability and reproducibility are two important factors that need to be considered when evaluating the performance of a biosensor. Repeatability refers to the ability of the biosensor to produce the same results when it is used to measure the same sample multiple times (intra and interday precision). Regarding the precision of the method based on new sensor, both intra and inter-day precision were evaluated by determining two different concentrations of capsule samples and one urine and one serum samples in triplicates within the same day and on three consecutive days. The acquired data were processed and the values of % relative standard deviation assured the high precision of the proposed biosensor as presented in Table 2. Reproducibility refers to the ability of the biosensor to produce the same results when it is used by different operators or in different laboratories. And the results of the reproducibility of the method based on a biosensor was introduced in Table 3.. The results of the proposed method is in good agreement with those of the existing methods in the literature, Table 4. This suggests that the proposed method is reliable and can be used for the determination of Molnupiravir in a variety of samples.

Conclusion

The proposed analytical method based on the use of a compound Fe-GA MOF is simple, economical and can be successfully applied for accurate and sensitive determination of Molnupiravir in various matrices including dosage forms, urine and serum. The Fe-GA MOF is more sensitive to Molnupiravir in DMSO with an LOD of 2.24×10^{-9} mol/L if compared with other published determination methods, Table 4. The Fe-GA MOF complex is a promising new tool for the determination of molnupiravir. It is easy to use, economical and sensitive. It can be used

Table 3
Results of reproducibility study.

		Results obtained by thermo scientific spectrofluorometer lab. 1 (n = 3)		Results obtained by FS5 spectrofluorometer lab. 2 (n = 3)	
Samples	standard method*	Proposed method	Pure MOL recovered (Percent ± SD)	Proposed method	Pure MOL recovered (Percent ± SD)
MOL 200 mg per capsule	0.10	0.102	102.0 ± 1.25	0.101	101.0 ± 1.05
[MOL] × 10^{-7} mol/L	1.00	0.980	98.00 ± 1.45	0.995	99.50 ± 1.05
Urine sample (real) μmol	0.53	0.525	99.0 ± 1.2	0.528	99.62 ± 0.7
Serum sample (real) μmol	0.52	0.514	98.8 ± 1.80	0.519	99.8 ± 0.50

Table 4
A comparison between literature and the developed method.

Method	Mobile Phase	Stationary phase	Linear range μg/mL	Ref.
LC-MS-MS	1 mM Ammonium acetate in water (pH4.3) and 1 mM Ammonium acetate in acetonitrile	polar Atlantis C18 column	2.5–5000	[85]
LC	ammonium formate and ACN	Waters Xselect HSS T3 (75 × 4.6 mm, 2.5 μm)	————————	[86]
RP-HPLC-PDA	ACN:water (20:80 v/v)	Discovery® HS C18 Column (75 × 4.6 mm, 3 μm)	0.1–60.0	[87]
RP-HPLC-UV	20 mM phosphate buffer pH 2.5: acetonitrile; 80:20, v/v%	Inertsil C_{18}, column (150 × 4.6 mm, 5 μm)	0.2–80.0	[88]
Fluorescence/ MOF method	——	———	0.1 – 0.001	The developed method

to determine Molnupiravir in a variety of matrices, including urine and serum dosage forms. The Fe-GA MOF complex is a valuable addition to an analytical chemist's toolkit.

CRediT authorship contribution statement

Huda M.Younis: Funding acquisition, Investigation, Methodology, Validation, Visualization. **A.O.Youssef:** Supervision, Validation, Visualization, Writing – original draft, Writing – review & editing. **Said M. El-Sheikh:** Investigation, Methodology, Project administration, Resources, Software, Supervision. **Sheta M.Sheta:** Investigation, Methodology, Project administration, Resources, Software, Supervision. **Mohamed S.Attia:** Conceptualization, Data curation, Formal analysis, Writing – original draft, Writing – review & editing.

Declaration of Competing Interest

The authors declare that they have no known competing financial interests or personal relationships that could have appeared to influence the work reported in this paper.

Data availability

No data was used for the research described in the article.

References

[1] R. Abdelnabi, C.S. Foo, S. De Jonghe, P. Maes, B. Weynand, J. Neyts, Molnupiravir Inhibits Replication of the Emerging SARS-CoV-2 Variants of Concern in a Hamster Infection Model, J Infect Dis 224 (5) (2021) 749–753.
[2] C.J. Gordon, E.P. Tchesnokov, R.F. Schinazi, M. Götte, Molnupiravir promotes SARS-CoV-2 mutagenesis via the RNA template, J. Biol. Chem. 297 (1) (2021), 100770.
[3] F. Graham, Daily briefing: Inside Merck's COVID drug, molnupiravir, Nature (2021).
[4] W. Holman, W. Holman, S. McIntosh, W. Painter, G. Painter, J. Bush, et al., Accelerated first-in-human clinical trial of EIDD-2801/MK-4482 (molnupiravir), a ribonucleoside analog with potent antiviral activity against SARS-CoV-2, Trials 22 (1) (2021) 561.
[5] R. Abdelnabi, C.S. Foo, S.J.F. Kaptein, X. Zhang, T.N.D. Do, L. Langendries, L. Vangeel, J. Breuer, J. Pang, R. Williams, V. Vergote, E. Heylen, P. Leyssen, K. Dallmeier, L. Coelmont, A.K. Chatterjee, R. Mols, P. Augustijns, S. De Jonghe, D. Jochmans, B. Weynand, J. Neyts, The combined treatment of Molnupiravir and Favipiravir results in a potentiation of antiviral efficacy in a SARS-CoV-2 hamster infection model, EBioMedicine 72 (2021), 103595.
[6] M. Imran, M. Kumar Arora, S.M.B. Asdaq, S.A. Khan, S.I. Alaqel, M.K. Alshammari, M.M. Alshehri, A.S. Alshrari, A. Mateq Ali, A.M. Al-shammeri, B.D. Alhazmi, A. A. Harshan, M.T. Alam, A. Abida, Discovery, Development, and Patent Trends on Molnupiravir: A Prospective Oral Treatment for COVID-19, Molecules 26 (19) (2021) 5795.
[7] F. Kabinger, C. Stiller, J. Schmitzová, C. Dienemann, G. Kokic, H.S. Hillen, C. Höbartner, P. Cramer, Mechanism of molnupiravir-induced SARS-CoV-2 mutagenesis, Nat. Struct. Mol. Biol. 28 (9) (2021) 740–746.
[8] S.H. Khoo, R. Fitzgerald, T. Fletcher, S. Ewings, T. Jaki, R. Lyon, N. Downs, L. Walker, O. Tansley-Hancock, W. Greenhalf, C. Woods, H. Reynolds, E. Marwood, P. Mozgunov, E. Adams, K. Bullock, W. Holman, M.D. Bula, J.L. Gibney, G. Saunders, A. Corkhill, C. Hale, K. Thorne, J. Chiong, S. Condie, H. Pertinez, W. Painter, E. Wrixon, L. Johnson, S. Yeats, K. Mallard, M. Radford, K. Fines, V. Shaw, A. Owen, D.G. Lalloo, M. Jacobs, G. Griffiths, Optimal dose and safety of molnupiravir in patients with early SARS-CoV-2: a Phase I, open-label, dose-escalating, randomized controlled study, J. Antimicrob. Chemother. 76 (12) (2021) 3286–3295.
[9] E. Mahase, Covid-19: Molnupiravir reduces risk of hospital admission or death by 50% in patients at risk, MSD reports. Bmj. 375 (2021), n2422.
[10] B. Malone, E.A. Campbell, Publisher Correction: Molnupiravir: coding for catastrophe, Nat. Struct. Mol. Biol. 28 (11) (2021) 955.
[11] G.P. Ahlqvist, C.P. McGeough, C. Senanayake, J.D. Armstrong, A. Yadaw, S. Roy, S. Ahmad, D.R. Snead, T.F. Jamison, Progress Toward a Large-Scale Synthesis of Molnupiravir (MK-4482, EIDD-2801) from Cytidine, ACS Omega 6 (15) (2021) 10396–10402.
[12] B. Malone, E.A. Campbell, Molnupiravir: coding for catastrophe, Nat. Struct. Mol. Biol. 28 (9) (2021) 706–708.
[13] L. Menéndez-Arias, Decoding molnupiravir-induced mutagenesis in SARS-CoV-2, J. Biol. Chem. 297 (1) (2021), 100867.
[14] G.R. Painter, M.G. Natchus, O. Cohen, W. Holman, W.P. Painter, Developing a direct acting, orally available antiviral agent in a pandemic: the evolution of molnupiravir as a potential treatment for COVID-19, Curr. Opin. Virol. 50 (2021) 17–22.
[15] J. Reina, Plitidepsin, an inhibitor of the cell elongation factor eEF1a, and molnupiravir an analogue of the ribonucleoside cytidine, two new chemical compounds with intense activity against SARS-CoV-2, Revista espanola de quimioterapia : publicacion oficial de la Sociedad Espanola de Quimioterapia. 34 (5) (2021) 402–407.
[16] Fischer W, Eron JJ, Holman W, Cohen MS, Fang L, Szewczyk LJ, et al. Molnupiravir, an Oral Antiviral Treatment for COVID-19. medRxiv : the preprint server for health sciences. 2021.
[17] W.P. Painter, W. Holman, J.A. Bush, F. Almazedi, H. Malik, N. Eraut, et al., Human Safety, Tolerability, and Pharmacokinetics of Molnupiravir, a Novel Broad-Spectrum Oral Antiviral Agent with Activity Against SARS-CoV-2, Antimicrob. Agents Chemother. (2021).
[18] Y. Wang, P. Li, K. Solanki, Y. Li, Z. Ma, M.P. Peppelenbosch, M.S. Baig, Q. Pan, Viral polymerase binding and broad-spectrum antiviral activity of molnupiravir against human seasonal coronaviruses, Virology 564 (2021) 33–38.
[19] C. Willyard, How antiviral pill molnupiravir shot ahead in the COVID drug hunt, Nature (2021).
[20] K. Rosenke, F. Hansen, B. Schwarz, F. Feldmann, E. Haddock, R. Rosenke, K. Barbian, K. Meade-White, A. Okumura, S. Leventhal, D.W. Hawman, E. Ricotta,

C.M. Bosio, C. Martens, G. Saturday, H. Feldmann, M.A. Jarvis, Orally delivered MK-4482 inhibits SARS-CoV-2 replication in the Syrian hamster model, Nat. Commun. 12 (1) (2021).
[21] A. Amara, S.D. Penchala, L. Else, C. Hale, R. FitzGerald, L. Walker, et al., The development and validation of a novel LC-MS/MS method for the simultaneous quantification of Molnupiravir and its metabolite ss-d-N4-hydroxycytidine in human plasma and saliva, J. Pharm. Biomed. Anal. 206 (2021), 114356.
[22] L. Gutierrez-Arzaluz, J. Jia, C. Gu, J. Czaban-Jozwiak, J. Yin, O. Shekhah, O. M. Bakr, M. Eddaoudi, O.F. Mohammed, Directional Exciton Migration in Benzoimidazole-Based MetalOrganic Frameworks, J. Phys. Chem. Lett. 12 (2021) 4917–4927.
[23] H. Jiang, D. Alezi, M. Eddaoudi, A Reticular Chemistry Guide for the Design of Periodic Solids, Nat. Rev. Mater. 6 (2021) 466–487.
[24] S. Zhou, O. Shekhah, J. Jia, J. Czaban-Jóźwiak, P.M. Bhatt, A. Ramírez, J. Gascon, M. Eddaoudi, Electrochemical Synthesis of Continuous Metal-Organic Framework Membranes for Separation of Hydrocarbons, Nat. Energy 6 (2021) 882–891.
[25] J. Perego, I. Villa, A. Pedrini, E.C. Padovani, R. Crapanzano, A. Vedda, C. Dujardin, C.X. Bezuidenhout, S. Bracco, P.E. Sozzani, A. Comotti, L. Gironi, M. Beretta, M. Salomoni, N. Kratochwil, S. Gundacker, E. Auffray, F. Meinardi, A. Monguzzi, Composite Fast Scintillators based on High-Z Fluorescent Metal-Organic Framework Nanocrystals, Nat. Photonics 15 (5) (2021) 393–400.
[26] Y. Xiao, C. Chen, Y. Wu, Y. Yin, H. Wu, H. Li, Y. Fan, J. Wu, S. Li, X. Huang, W. Zhang, B. Zheng, F. Huo, Fabrication of Two-Dimensional Metal−Organic Framework Nanosheets through Crystal Dissolution−Growth Kinetics, ACS Appl. Mater. Interfaces 14 (2022) 7192–7199.
[27] D. Gao, J.-H. Chen, S. Fang, T. Ma, X.-H. Qiu, J.-G. Ma, Q. Gu, P. Cheng, Simultaneous Quantitative Recognition of All Purines Including N6-Methyladenine Via the Host-Guest Interactions on a Mn-MOF, Matter. 4 (2021) 1001–1016.
[28] J. Su, W. He, X.-M. Li, L. Sun, H.-Y. Wang, Y.-Q. Lan, M. Ding, J.-L. Zuo, High Electrical Conductivity in a 2D MOF with Intrinsic Superprotonic Conduction and Interfacial Pseudo-capacitance, Matter. 2 (2020) 711–722.
[29] R. Haldar, L. Heinke, C. Woll, Advanced Photoresponsive Materials Using the Metal-Organic Framework Approach, Adv. Mater. 32, No. e1905227 (2020).
[30] A.M. Rice, C.R. Martin, V.A. Galitskiy, A.A. Berseneva, G.A. Leith, N.B. Shustova, Photophysics Modulation in Photoswitchable Metal-Organic Frameworks, Chem. Rev. 120 (2020) 8790–8813.
[31] X. Li, S. Surendran Rajasree, J. Yu, P. Deria, The Role of Photoinduced Charge Transfer for Photocatalysis, Photoelectrocatalysis and Luminescence Sensing in Metal-Organic Frameworks, Dalton Trans. 49 (2020) 12892–12917.
[32] Y. Zhao, H. Zeng, X.W. Zhu, W. Lu, D. Li, Metal-Organic Frameworks as Photoluminescent Biosensing Platforms: Mechanisms and Applications, Chem. Soc. Rev. 50 (2021) 4484–4513.
[33] Y. Zhao, J. Wang, W. Zhu, L. Liu, R. Pei, The Modulation Effect of Charge Transfer on Photoluminescence in Metal-Organic Frameworks, Nanoscale 13 (2021) 4505–4511.
[34] T. Islamoglu, Z. Chen, M.C. Wasson, C.T. Buru, K.O. Kirlikovali, U. Afrin, M. R. Mian, O.K. Farha, Metal-Organic Frameworks against Toxic Chemicals, Chem. Rev. 120 (2020) 8130–8160.
[35] H.Y. Li, S.N. Zhao, S.Q. Zang, J. Li, Functional MetalOrganic Frameworks as Effective Sensors of Gases and Volatile Compounds, Chem. Soc. Rev. 49 (2020) 6364–6401.
[36] Y.u. Zhang, X. Qu, B. Yan, A Visual Logic Alarm Sensor for Diabetic Patients Towards Diabetic Polyneuropathy Based on a Metal-Organic Framework Functionalized by Dual-Cation Exchange, J. Mater. Chem. C 9 (10) (2021) 3440–3446.
[37] S.-R. Zhang, G.-J. Xu, W. Xie, Y.-H. Xu, Z.-M. Su, A Luminescent Metal-Organic Framework with Mixed-Linker Strategy for White-Light-Emitting by Iridium-Complex Encapsulation, Inorg. Chem. Commun. 123 (2021), 108359.
[38] X.D. Ying, J.X. Chen, D.Y. Tu, Y.C. Zhuang, D. Wu, L. Shen, Tetraphenylpyrazine-Based Luminescent Metal-Organic Framework for Chemical Sensing of Carcinoids Biomarkers, ACS Appl. Mater. Interfaces 13 (2021) 6421–6429.
[39] X. Wang, M. Lei, T. Zhang, Q. Zhang, R. Zhang, M. Yang, A Water-Stable Multi-Responsive Luminescent Zn-MOF Sensor for Detecting TNP, NZF and Cr2O7(2–) in Aqueous Media, Dalt. Trans. 50 (2021) 3816–3824.
[40] S. Yuvaraja, S.G. Surya, V. Chernikova, M.T. Vijjapu, O. Shekhah, P.M. Bhatt, S. Chandra, M. Eddaoudi, K.N. Salama, Realization of an Ultrasensitive and Highly Selective OFET NO2 Sensor: The Synergistic Combination of PDVT-10 Polymer and Porphyrin-MOF, ACS Appl. Mater. Interfaces 12 (2020) 18748–18760.
[41] M.A. Andres, M.T. Vijjapu, S.G. Surya, O. Shekhah, K.N. Salama, C. Serre, M. Eddaoudi, O. Roubeau, I. Gascon, Methanol and Humidity Capacitive Sensors Based on Thin Films of MOF Nanoparticles, ACS Appl. Mater. Interfaces 12 (2020) 4155–4162.
[42] S. Wu, H. Min, W. Shi, P. Cheng, Multicenter Metal-Organic Framework-Based Ratiometric Fluorescent Sensors, Adv. Mater. 32, No. e1805871 (2020).
[43] Y. Li, J. Liu, Z. Wang, J. Jin, Y. Liu, C. Chen, Z. Tang, Optimizing Energy Transfer in Nanostructures Enables In Vivo Cancer Lesion Tracking via Near-Infrared Excited Hypoxia Imaging, Adv. Mater. 32, No. e1907718 (2020).
[44] M. Zeng, A. Ren, W. Wu, Y. Zhao, C. Zhan, J. Yao, Lanthanide MOFs for Inducing Molecular Chirality of Achiral Stilbazolium with Strong Circularly Polarized Luminescence and Efficient Energy Transfer for Color Tuning, Chem. Sci. 11 (2020) 9154–9161.
[45] J. Yu, R. Anderson, X. Li, W. Xu, S. Goswami, S.S. Rajasree, K. Maindan, D. A. Gomez-Gualdron, P. Deria, Improving Energy Transfer within Metal-Organic Frameworks by Aligning Linker Transition Dipoles along the Framework Axis, J. Am. Chem. Soc. 142 (2020) 11192–11202.
[46] H. Wu, M. Li, C. Sun, X. Wang, Z. Su, Luminescent MetalOrganic Frameworks Encapsulating Polycyclic Aromatic Hydrocarbons for Energy Transfer, Dalton Trans. 49 (2020) 5087–5091.
[47] A. Afzalinia, M. Mirzaee, Ultrasensitive Fluorescent miRNA Biosensor Based on a "Sandwich" Oligonucleotide Hybridization and Fluorescence Resonance Energy Transfer Process Using an Ln(III)- MOF and Ag Nanoparticles for Early Cancer Diagnosis: Application of Central Composite Design, ACS Appl. Mater. Interfaces 12 (2020) 16076–16087.
[48] G.E. Gomez, R. Marin, A.N. Carneiro Neto, A.M.P. Botas, J. Ovens, A.A. Kitos, M. C. Bernini, L.D. Carlos, G.J.A.A. Soler-Illia, M. Murugesu, Tunable Energy-Transfer Process in Heterometallic MOF Materials Based on 2,6-Naphthalenedicarboxylate: Solid-State Lighting and Near-Infrared Luminescence Thermometry, Chem. Mater. 32 (2020) 7458–7468.
[49] C. Xia, Y. Xu, M.M. Cao, Y.P. Liu, J.F. Xia, D.Y. Jiang, G.H. Zhou, R.J. Xie, D. F. Zhang, H.L. Li, A Selective and Sensitive Fluorescent Probe for Bilirubin in Human Serum based on Europium(III) Post-Functionalized Zr(IV)-Based MOFs, Talanta 212 (2020), 120795.
[50] J.C. Yin, Z. Chang, N. Li, J. He, Z.X. Fu, X.H. Bu, Efficient Regulation of Energy Transfer in a Multicomponent Dye-Loaded MOF for White-Light Emission Tuning, ACS Appl. Mater. Interfaces 12 (2020) 51589–51597.
[51] Z. Wang, C. Wang, Excited State Energy Transfer in MetalOrganic Frameworks, Adv. Mater. 33 (2021) 2005819.
[52] H.A. AlGhamdi, Y.M. AlZahrani, S. Alharthi, M.S. Mohy-Eldin, E.H. Mohamed, S. A. Mahmoud, M.S. Attia, Novel sensor for the determination of CA 15–3 in serum of breast cancer patients based on Fe–gallic acid complex doped in modified cellulose polymer thin films, **RSC Adv.** 13 (31) (2023) 21769–21780.
[53] Z. Bao, J. Wang, Z. Zhang, H. Xing, Q. Yang, Y. Yang, H. Wu, R. Krishna, W. Zhou, B. Chen, Molecular Sieving of Ethane from Ethylene through the Molecular Cross-Section Size Differentiation in Gallate-based Metal-Organic Frameworks, Angew. Chem. 130 (2018) 16252–16257.
[54] A. Ponce, L.B. Brostoff, S.K. Gibbons, P. Zavalij, C. Viragh, J. Hooper, S. Alnemrat, K.J. Gaskell, B. Eichhorn, Elucidation of the Fe(III) Gallate Structure in Historical Iron Gall Ink, Anal. Chem. 88 (2016) 5152–5158.
[55] M. A. Rahim, K. Kempe, M. Mullner, H. Ejima, Y. Ju, ¨M. P. van Koeverden, T. Suma, J. A. Braunger, M. G. Leeming, B. F. Abrahams and F. Caruso, Surface-Confined Amorphous Films from Metal-Coordinated.
[56] Z. Chen, H. Jiang, M. Li, M. O'Keeffe, M. Eddaoudi, Reticular Chemistry 3.2: Typical Minimal Edge-Transitive Derived and Related Nets for the Design and Synthesis of Metal-Organic Frameworks, Chem. Rev. 120 (2020) 8039–8065.
[57] J.-X. Wang, H. Zhang, L.-Y. Niu, X. Zhu, Y.-F. Kang, R. Boulatov, Q.-Z. Yang, Organic Composite Crystal with Persistent Room-Temperature Luminescence Above 650 nm by Combining Triplet-Triplet Energy Transfer with Thermally Activated Delayed Fluorescence, CCS. Chem. 2 (2020) 1391–1398.
[58] H. Niu, Y. Zheng, ab Saihua Wang, Sijing He and Yaqi Cai, Stable hierarchical microspheres of 1D Fe–gallic acid MOFs for fast and efficient Cr(VI) elimination by a combination of reduction, metal substitution and coprecipitation, J. Mater. Chem. A 5 (2017) 16600–16604.
[59] B. Gui, X. Liu, G. Yu, W. Zeng, A. Mal, S. Gong, C. Yang, C. Wang, Tuning of Förster Resonance Energy Transfer in MetalOrganic Frameworks: Toward Amplified Fluorescence Sensing, CCS. Chem. 3 (2021) 2054–2062.
[60] T. Manjuraj, G. Krishnamurthy, Y.D. Bodke, H.S. Bhojya Naik, J. Mol. Struct. 1148 (2017) 231–237.
[61] R. Sacourbaravi, Z. Ansari-Asl, M. Kooti, V. Nobakht, E. Darabpour, Fabrication of Ag NPs/Zn-MOF Nanocomposites and Their Application as Antibacterial Agents, J. Inorg. Organomet. Polym. 30 (11) (2020) 4615–4621.
[62] M.D. Allendorf, C.A. Bauer, R.K. Bhakta, R.J.T. Houk, Chem. Soc. Rev. 38 (2009) 1330.
[63] (a) J. Rocha, L.D. Carlos, F.A. Almeida Paz, D. Ananias, Chem. Soc. Rev. 40 (2011) 926;
(b) Y.J. Cui, Y.F. Yue, G.D. Qian, B.L. Chen, Chem. Rev. 112 (2012) 1126;
(c) F.A. Almeida Paz, J. Klinowski, S.M.F. Vilela, J.P.C. Tome, J.A.S. Cavaleiro, J. Rocha, Chem. Soc. Rev. 41 (2012) 1088;
(d) M. Pan, W.M. Liao, S.Y. Yin, S.S. Sun, C.Y. Su, Chem. Rev. 118 (2018) 8889.
[64] M. Zheng, H. Tan, Z. Xie, L. Zhang, X. Jing, Z. Sun, A.C.S. Appl, Mater. Interfaces 5 (2013) 1078–1108.
[65] P.J. Saines, H.-H.-M. Yeung, J.R. Hester, A.R. Lennie, A.K. Cheetham, Detailed investigations of phase transitions and magnetic structure in Fe(III), Mn(II), Co(II) and Ni(II) 3,4,5-trihydroxybenzoate (gallate) dihydrates by neutron and X-ray diffraction, Dalton Trans. 40 (2011) 6401–6410.
[66] R.K. Feller, A.K. Cheetham, Fe(III), Mn(II), Co(II), and Ni(II) 3,4,5-trihydroxybenzoate (gallate) dihydrates; a new family of hybrid framework materials, Solid State Sci. 8 (2006) 1121–1125.
[67] J. Wang, L. Li, L. Guo, Y. Zhao, D. Xie, Z. Zhang, Q. Yang, Y. Yang, Z. Bao, Q. Ren, Adsorptive Separation of Acetylene from Ethylene in Isostructural Gallate-Based Metal-Organic Frameworks, Chem Eur J 25 (2019) 15516–15524.
[68] M.S. Attia, A.O. Youssef, Z.A. Khan, M.N. Abou-Omar, Talanta 186 (2018) 36–43.
[69] M.S. Attia, M.H. Khalil, M.S.A. Abdel-Mottaleb, M.B. Lukyanova, Y.A. Alekseenko, B. Lukyanov, Int. J. Photoenergy 2006 (2006) 1–9.
[70] M.S. Attia, A.O. Youssef, A.A. Essawy, Anal. Methods 4 (2012) 2323–2328.
[71] M.S. Attia, K. Ali, M. El-Kemary, W.M. Darwish, Talanta 201 (2019) 185–193.
[72] M.S. Attia, W.H. Mahmoud, A.O. Youssef, M.S. Mostafa, J. Fluoresc. 21 (2011) 2229–2235.
[73] M.S. Attia, M.N. Ramsis, L.H. Khalil, S.G. Hashem, J. Fluoresc. 22 (2012) 779–788.
[74] M.S. Attia, W.H. Mahmoud, M.N. Ramsis, L.H. Khalil, A.M. Othman, S.G. Hashem, M.S. Mostafa, J. Fluoresc. 21 (2011) 1739–1748.

[75] M.S. Attia, A.M. Othman, E. Elraghi, H.Y. Aboul-Enein, J. Fluoresc. 21 (2011) 739–745.
[76] A.A. Elabd, M.S. Attia, J. Lumines. 169 (2016) 313–318.
[77] M.S. Attia, E. Bakir, A.A. Abdel-Aziz, M.S.A. Abdel-Mottaleb, Talanta 84 (2011) 27–33.
[78] M.S. Abdel-Wahed, A.S. El-Kalliny, M.I. Badawy, M.S. Attia, T.A. Gad-Allah, Chem. Eng. J. 382 (2020), 122936.
[79] M.S. Attia, S.A. Elsaadany, K.A. Ahmed, M.M. El-Molla, M.S.A. Abdel-Mottaleb, J. Fluoresc. 25 (2015) 119–125.
[80] S.G. Hashem, M.M. Elsaady, H.G. Afify, M. El-Kemary, M.S. Attia, Talanta 199 (2019) 89–96.
[81] M.S.A. Abdel-Mottaleb, M. Saif, M.S. Attia, M.M. Abo-Aly, S.N. Mobarez, Photochem. Photobio. Sci. 17 (2018) 221–230.
[82] Omer, W.E., El-Kemary, M.A., Elsaady, M.M., ...Gouda, A.A., Attia, M.S., ACS Omega 5(2020) 5629–5637.
[83] L.M. Abdullah, M.S. Attia, M.S.A. Abdel-Mottaleb, Egy. J. Chem. 62 (2019) 247–255.
[84] ICH. Validation of Analytical Procedures: Text and Methodology, Q2(R1), Complementary Guideline on Methodology. ICH, London, November 1996. 2005.
[85] S.-R. Zhang, G.-J. Xu, W. Xie, Y.-H. Xu, Z.-M. Su, A Luminescent Metal-Organic Framework with Mixed-Linker Strategy for White-Light-Emitting by Iridium-Complex Encapsulation, Inorg. Chem. Commun. 123 (2021), 108359.
[86] A.M. Annadi, N.M. El Zahar, N. El-Din Abdel-Sattar, S.A. Mahmoud, M.S. Attia, Development and validation of molnupiravir assessment in bulk powder and pharmaceutical formulation by the RP-HPLC-UV method, RSC Adv. 12 (53) (2022) 34512–34519.
[87] X. Wang, M. Lei, T. Zhang, Q. Zhang, R. Zhang, M. Yang, A Water-Stable Multi-Responsive Luminescent Zn-MOF Sensor for Detecting TNP, NZF and Cr2O7(2–) in Aqueous Media, Dalt. Trans. 50 (2021) 3816–3824.
[88] Abdelaziz M. Annadi, Noha M. El Zahar, Nour El-Din A. Abdel-Sattar, Ekram H. Mohamed, Safwat A. Mahmoud and Mohamed S. Attia, Development and validation of molnupiravir assessment in bulk powder and pharmaceutical formulation by the RP-HPLC-UV method. RSC Adv. 12 (2022)34512–34519.